Abrupt rise in atmospheric CO2 at the onset of the Bølling/Allerød: in-situ ice core data versus true atmospheric signals

P. Köhler, G. Knorr, D. Buiron, A. Lourantou, J. Chappellaz

Clim. Past, 7, 473–486, 2011
www.clim-past.net/7/473/2011/
doi:10.5194/cp-7-473-2011

Climate of the Past

Abrupt rise in atmospheric CO_2 at the onset of the Bølling/Allerød: in-situ ice core data versus true atmospheric signals

P. Köhler[1], **G. Knorr**[1,2], **D. Buiron**[3], **A. Lourantou**[3,*], **and J. Chappellaz**[3]

[1]Alfred Wegener Institute for Polar and Marine Research (AWI), P.O. Box 120161, 27515 Bremerhaven, Germany
[2]School of Earth and Ocean Sciences, Cardiff University, Cardiff, Wales, UK
[3]Laboratoire de Glaciologie et Géophysique de l'Environnement, (LGGE, CNRS, Université Joseph Fourier-Grenoble), 54b rue Molière, Domaine Universitaire BP 96, 38402 St. Martin d'Hères, France
[*]now at: Laboratoire d'Océanographie et du Climat (LOCEAN), Institut Pierre Simon Laplace, Université P. et M. Curie (UPMC), Paris, France

Received: 24 June 2010 – Published in Clim. Past Discuss.: 11 August 2010
Revised: 15 March 2011 – Accepted: 24 March 2011 – Published: 4 May 2011

Abstract. During the last glacial/interglacial transition the Earth's climate underwent abrupt changes around 14.6 kyr ago. Temperature proxies from ice cores revealed the onset of the Bølling/Allerød (B/A) warm period in the north and the start of the Antarctic Cold Reversal in the south. Furthermore, the B/A was accompanied by a rapid sea level rise of about 20 m during meltwater pulse (MWP) 1A, whose exact timing is a matter of current debate. In-situ measured CO_2 in the EPICA Dome C (EDC) ice core also revealed a remarkable jump of 10 ± 1 ppmv in 230 yr at the same time. Allowing for the modelled age distribution of CO_2 in firn, we show that atmospheric CO_2 could have jumped by 20–35 ppmv in less than 200 yr, which is a factor of 2–3.5 greater than the CO_2 signal recorded in-situ in EDC. This rate of change in atmospheric CO_2 corresponds to 29–50% of the anthropogenic signal during the last 50 yr and is connected with a radiative forcing of 0.59–0.75 W m^{-2}. Using a model-based airborne fraction of 0.17 of atmospheric CO_2, we infer that 125 Pg of carbon need to be released into the atmosphere to produce such a peak. If the abrupt rise in CO_2 at the onset of the B/A is unique with respect to other Dansgaard/Oeschger (D/O) events of the last 60 kyr (which seems plausible if not unequivocal based on current observations), then the mechanism responsible for it may also have been unique. Available $\delta^{13}CO_2$ data are neutral, whether the source of the carbon is of marine or terrestrial origin. We therefore hypothesise that most of the carbon might have been activated as a consequence of continental shelf flooding during MWP-1A. This potential impact of rapid sea level rise on atmospheric CO_2 might define the point of no return during the last deglaciation.

Correspondence to: P. Köhler
(peter.koehler@awi.de)

1 Introduction

Measurements of CO_2 over Termination I (20–10 kyr BP) from the EPICA Dome C (EDC) ice core (Monnin et al., 2001; Lourantou et al., 2010) (Fig. 1b) are temporally higher resolved and more precise than CO_2 records from other ice cores (Smith et al., 1999; Ahn et al., 2004). They have an uncertainty (1σ) of 1 ppmv or less (Monnin et al., 2001; Lourantou et al., 2010). In these in-situ measured data in EDC, CO_2 abruptly rose by 10 ± 1 ppmv between 14.74 and 14.51 kyr BP on the most recent ice core age scale (Lemieux-Dudon et al., 2010). This abrupt CO_2 rise is therefore synchronous with the onset of the Bølling/Allerød (B/A) warm period in the North (Steffensen et al., 2008), the start of the Antarctic Cold Reversal in the South (Stenni et al., 2001), as well as abrupt rises in the two other greenhouse gases CH_4 (Spahni et al., 2005) and N_2O (Schilt et al., 2010). Furthermore, the B/A is accompanied by a rapid sea level rise of about 20 m during meltwater pulse (MWP) 1A (Peltier and Fairbanks, 2007), whose exact timing is matter of current debate (e.g. Hanebuth et al., 2000; Kienast et al., 2003; Stanford et al., 2006; Deschamps et al., 2009).

However, atmospheric gases trapped in ice cores are not precisely recording one point in time but average over decades to centuries, mainly depending on their

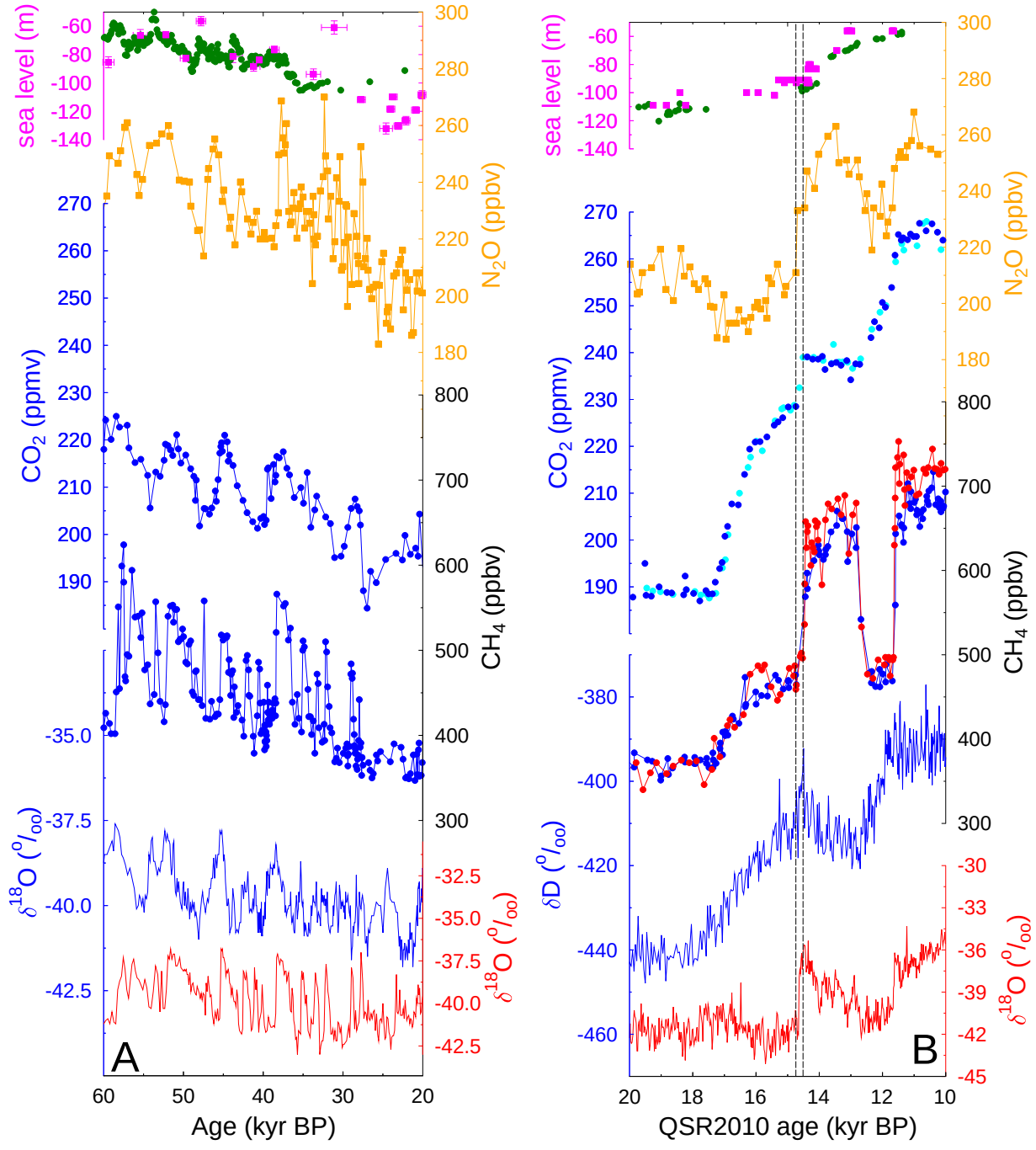

Fig. 1. Climate records during MIS 3 and Termination I. From top to bottom: relative sea level, N_2O, CO_2, CH_4 and isotopic temperature proxies (δD or $\delta^{18}O$) from Antarctica (blue) and Greenland (red). **(A)** MIS 3 data from the Byrd (CO_2, CH_4, $\delta^{18}O$), GISP2 (Ahn and Brook, 2008) and Talos Dome ice cores (N_2O) (Schilt et al., 2010). Sea level from a compilation (magenta) based on coral reef terraces (Thompson and Goldstein, 2007) and the synthesis (green) from the Red Sea method (Siddall et al., 2008). Age model of Byrd and GISP2 as in Ahn and Brook (2008) and Talos Dome data on the TALDICE-1 age scale (Buiron et al., 2011). **(B)** Termination I data from the EDC (blue, cyan: CO_2, CH_4, δD), Talos Dome (N_2O) and NGRIP (red: CH_4, $\delta^{18}O$) ice cores (Monnin et al., 2001; Stenni et al., 2001; NorthGRIP-members, 2004; Lourantou et al., 2010; Schilt et al., 2010). Previous (Monnin et al., 2001) (blue) and new (Lourantou et al., 2010) (cyan) EDC CO_2 data. Sea level in from corals (green) on Barbados, U-Th dated and uplift-corrected (Peltier and Fairbanks, 2007), and coast line migration (magenta) on the Sunda Shelf (Hanebuth et al., 2000). In **(B)** sea level is plotted on an individual age scale, N_2O on TALDICE-1 age scale of Talos Dome (Buiron et al., 2011), and EDC and NGRIP data are plotted on the new synchronised ice core age scale QSR2010 (Lemieux-Dudon et al., 2010). Vertical lines in **(B)** mark the jump in CO_2 into the B/A as recorded in EDC.

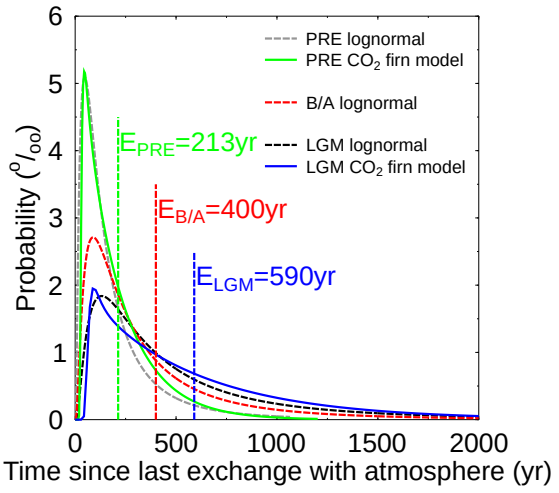

Fig. 2. Age distribution PDF of CO_2 as a function of climate state, here pre-industrial (PRE), Bølling/Allerød (B/A) and LGM conditions. Calculation with a firn densification model (Joos and Spahni, 2008) (solid lines, for PRE and LGM) and approximations of all three climate states by a log-normal function (broken lines). For all functions the expected mean values, or width E, are also given.

accumulation rate because of the movement of gases in the firn above the close-off depth and before its enclosure in gas bubbles in the ice. To infer the transfer signature of the true atmospheric CO_2 signal out of in-situ ice core CO_2 measurements, the latter has to be deconvoluted with the ice-core-specific age distribution probability density function (PDF). Based on a firn densification model (Joos and Spahni, 2008), this age distribution PDF describing the elapsed time since the last exchange of the CO_2 molecules with the atmosphere (Fig. 2) reveals for EDC a width of approximately 200 and 600 yr for climate conditions of pre-industrial times (PRE) and the Last Glacial Maximum (LGM), respectively. These wide age distributions implicate that the CO_2 measured in-situ, especially in ice cores with low accumulation rates (such as EDC), differs from the true atmospheric signal when CO_2 changes abruptly.

In the following we will deconvolve the atmospheric CO_2 signal connected with this abrupt rise in CO_2 measured in-situ in the EDC ice core, allowing for the age distribution PDF during the onset of the B/A. We furthermore use simulations of a global carbon cycle box model to develop and test a hypotheses which might explain the abrupt rise in atmospheric CO_2.

2 Methods

2.1 Age distribution PDF of CO_2

The age distributions PDF of CO_2 or CH_4 are functions of the climate state and the local site conditions of the ice core. In Fig. 2, the age distributions PDF of CO_2 in the EDC ice core for pre-industrial (PRE) and LGM conditions based on calculations with a firn densification model (Joos and Spahni, 2008) are shown. The resulting age distribution PDF for CO_2 can be approximated with reasonable accuracy ($r^2 = 90$–94%) by a log-normal function (Köhler et al., 2010b):

$$y = \frac{1}{x \cdot \sigma \cdot \sqrt{2\pi}} \cdot e^{-0.5\left(\frac{\ln(x)-\mu}{\sigma}\right)^2} \quad (1)$$

with x (yr) as the time elapsed since the last exchange with the atmosphere. This equation has two free parameters μ and σ. For simplcity, we have chosen $\sigma = 1$, which leads to an *expected value (mean)* E of the PDF of

$$E = e^{\mu+0.5} . \quad (2)$$

The *expected value* E is described as *width* of the PDF in the terminology of gas physics, a terminology which we will also use in the following. E should not be confused with the *most likely value* defined by the location of the maximum of the PDF.

Our choice to use a log-normal function (Eq. 1) for the age distribution PDF was motivated by the good representation of firn densification model output ($r^2 \geq 90\%$) and its dependency on only one free parameter, which can be obtained from models. Other approaches using, for example, a Green's function are also possible (see Trudinger et al., 2002, and references therein).

In the case of the CO_2 jump at 14.6 kyr BP, one has to consider that the atmospheric records are much younger than the surrounding ice matrix; indeed, the CO_2 jump is embedded between 473 and 480 m in glacial ice (Monnin et al., 2001; Lourantou et al., 2010) with low temperatures and low accumulation rates. However, from a model of firn densification which includes heat diffusion, it is known that the close-off of the gas bubbles in the ice matrix is not a simple function of the temperature of the surrounding ice (Goujon et al., 2003). Heat from the surface diffuses down to the close-off region in a few centuries, depending on site-specific conditions. This implies that atmospheric gases during the onset of the B/A were not trapped by conditions of either the LGM or the Antarctic Cold Reversal, but by some intermediate state. New calculations with this firn densification model (Goujon et al., 2003) give a width of the age distribution PDF $E_{B/A}$ of about 400 yr with a relative uncertainty (1σ) of 14% at the onset of the B/A (Fig. 3). The width E itself varies during the jump into the B/A between 380 and 420 yr; we therefore conservatively estimate $E_{B/A}$ to lie between 320 to 480 yr with our best-guess estimate of $E_{B/A} = 400$ yr in-between.

The performance of the applied gas age distribution PDF (Eq. 1) is tested with ice core CH_4 data for the time window of interest (Appendix A, Supplement). In summary, this test strongly suggests that the log-normal age distribution PDF does not introduce a systematic bias in the shape of the signal if applied onto a hypothetical atmospheric CO_2 record. It is

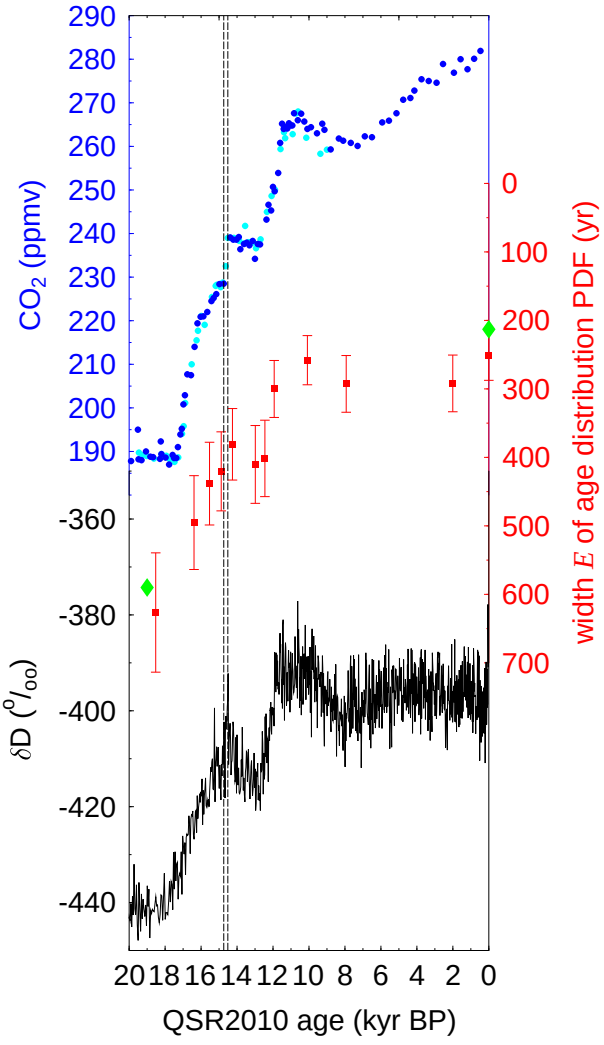

Fig. 3. Evolution of the width E of the age distribution PDF ($\pm 1\sigma$) during the last 20 kyr (red squares) calculated with a firn densification model including heat diffusion (Goujon et al., 2003). Green diamonds represent the results for the LGM and pre-industrial climate with another firn densification model (Joos and Spahni, 2008). Please note reverse y-axis. Top: EDC CO_2 (Monnin et al., 2001; Lourantou et al., 2010). Bottom: EDC δD data (Stenni et al., 2001). All records are on the new age scale QSR2010 (Lemieux-Dudon et al., 2010).

therefore justified to apply Eq. (1) to convolve the CO_2 signal which might be recorded in the EDC ice core.

2.2 Carbon cycle modelling

In order to determine how fast carbon injected into the atmosphere is taken up by the ocean, we used the carbon cycle box model BICYCLE (Köhler and Fischer, 2004; Köhler et al., 2005a, 2010b). The model version used here and its forcing over Termination I are described in detail in Lourantou et al. (2010). Furthermore, we tried to determine of which origin (terrestrial or marine) the carbon might have been by comparing the simulated and measured atmospheric $\delta^{13}CO_2$ fingerprint during the carbon release event. Similar approaches (identifying processes based on their $\delta^{13}C$ signature) were applied earlier for the discussion of the atmospheric $\delta^{13}CO_2$ record over the whole Termination I (Lourantou et al., 2010) and longer timescales (Köhler et al., 2010b). Here, we restrict the analysis to the question of whether the observed signal might be generated by terrestrial or marine processes only.

Briefly, BICYCLE consists of modules of the ocean (10 boxes distinguishing surface, intermediate and deep ocean in the Atlantic, Southern Ocean and Indo-Pacific), a globally averaged terrestrial biosphere (7 boxes), a homogeneously mixed one-box atmosphere, and a relaxation approach to account for carbonate compensation in the deep ocean (sediment-ocean interaction). The model calculates the temporal development of its prognostic variables over time as functions of changing boundary conditions, representing the climate forcing. These prognostic variables are (a) carbon (as dissolved inorganic carbon DIC in the ocean), (b) the carbon isotopes $\delta^{13}C$, $\Delta^{14}C$, and (c) additionally in the ocean total alkalinity, oxygen and phosphate. The terrestrial module accounts for different photosynthetic pathways (C_3 or C_4), which is relevant for the temporal development of the ^{13}C cycle.

Here, the model is equilibrated for 4000 yr for climate conditions typical before the onset of the B/A. The Atlantic meridional overturning circulation (AMOC) is in an off mode. Simulations with the AMOC in an on mode lead to a different background state of the carbon cycle (atmospheric pCO_2 is then 255 ppmv versus 223 ppmv in the off mode), but the amplitudes in the atmospheric CO_2 rise differ by less than 3 ppmv between both settings. Scenarios in which the AMOC amplifies precisely at the onset of the B/A warm period are not explicitly considered here, but are implicitly covered in the marine scenario. An amplification of the AMOC would lead to stadial/interstadial variations typical for the bipolar seesaw. Such behaviour was found for the onset of other D/O events in MIS 3 (Barker et al., 2010) during which CO_2 started to fall and not to rise as observed for the B/A. Based on this analogy, our working hypothesis is that the main processes connected with changes in the AMOC play a minor role for the abrupt rise in atmospheric CO_2 around 14.6 kyr BP (see Sect. 3.2 for details).

The simulated jump of CO_2 is generated by the injection of a certain amount of carbon into the atmosphere, while all other processes (ocean overturning, temperature, sea level, sea ice cover, marine productivity, terrestrial biosphere) are kept constant. The size of the injection is deduced from considerations on the airborne fraction and model simulations (see Sect. 3.1). The carbon is then brought with a constant injection flux in a time window of a different length (over either 50, 100, 150, 200, 250 or 300 yr) into the

atmosphere. Our best guess injection amplitude of 125 PgC corresponds to constant injection fluxes of 2.5 Pg C yr^{-1} (in 50 yr) to 0.42 Pg C yr^{-1} (in 300 yr) over the whole release period. The fastest injection (in 50 yr) with the largest annual flux has been motivated by the abruptness in the climate signals recorded in the NGRIP ice core (Steffensen et al., 2008). It is furthermore assumed that the injected carbon is either of terrestrial or marine origin. These two scenarios differ only in their carbon isotopic signature:

Terrestrial scenario: the δ^{13}C signature is based on a study with a global dynamical vegetation model (Scholze et al., 2003), which calculates a mean global isotopic fractionation of the terrestrial biosphere of 17.7‰ for the present day. We have to consider a larger fraction of C_4 plants during colder climates and lower atmospheric pCO_2 (Collatz et al., 1998), as found at the onset of the B/A. This implies that about 20 and 30% of the terrestrial carbon is of C_4 origin for present day and LGM, respectively (Köhler and Fischer, 2004). The significantly smaller isotopic fractionation during C_4 photosynthesis (about 5‰) in comparison to C_3 photosynthesis (about 20‰) (Lloyd and Farquhar, 1994) therefore reduces the global mean terrestrial fractionation to 16‰. With an atmospheric $\delta^{13}CO_2$ signature of about −6.5‰, the terrestrial biosphere has a mean δ^{13}C signature of −22.5‰.

Marine scenario: in this scenario we assume that old carbon from the deep ocean heavily depleted in δ^{13}C might upwell and outgas into the atmosphere. Today's values of oceanic δ^{13}C in the deep Pacific are about 0.0‰ (Kroopnick, 1985). From reconstructions (Oliver et al., 2010), it is known that during the LGM deep ocean δ^{13}C was on average about 0.5‰ smaller, thus $\delta^{13}C_{LGM}$=−0.5‰. During out-gassing, mainly in high latitudes, we consider a net isotopic fractionation of 8‰ (Siegenthaler and Münnich, 1981). This would lead to δ^{13}C=−8.5‰ in the carbon injected into the atmosphere if it were of marine origin.

The signals of simulated atmospheric CO_2 and $\delta^{13}CO_2$ plotted in the figures are derived by subtracting simulated CO_2 and $\delta^{13}CO_2$ of a reference run without carbon injections from our scenarios. The anomalies $\Delta(CO_2)$ and $\Delta(\delta^{13}CO_2)$ are then added to the starting point of the CO_2 jump ($\delta^{13}CO_2$ drop) into the B/A, which we define as 228 ppmv (−6.76‰) at 14.8 kyr BP. In doing so, existing equilibration trends (which will exist even for longer equilibration periods due to the sediment-ocean interaction) are eliminated. The simulated atmospheric CO_2 ($\delta^{13}CO_2$) at the end of the equilibration period was 223 ppmv (−6.54‰). Our modelling exercise is therefore only valid for an interpretation of the abrupt CO_2 rise of 10 ppmv in the in-situ data of EDC. The mismatch in CO_2 and $\delta^{13}CO_2$ between simulations and EDC data before 15 kyr BP and after 14.2 kyr BP, is therefore expected (Figs. 4b, 4d, 5b, 5d, 7).

3 Results and discussions

3.1 Assessing the size of the carbon injection

We first estimate roughly the amount of carbon necessary to be injected as CO_2 into the atmosphere to produce a long-term jump of 10 ppmv using the airborne fraction f. The long-term (centuries to millennia) airborne fraction f of CO_2 can be approximated from the buffer or Revelle factor (RF) of the ocean on atmospheric pCO_2 rise. The present day mean surface ocean Revelle factor (Sabine et al., 2004a) is about 10. With

$$\mathrm{RF} = \frac{\Delta pCO_2 / pCO_2}{\Delta \mathrm{DIC}/\mathrm{DIC}} \tag{3}$$

and the content of C at the beginning of the B/A in the atmosphere ($C_A = 500$ Pg C ≈ 235 ppmv) and in the ocean ($C_O = 37\,500$ Pg C = 75· C_A) it is

$$f = \frac{\Delta pCO_2}{\Delta pCO_2 + \Delta \mathrm{DIC}} = \frac{1}{1+\frac{75}{\mathrm{RF}}} = 0.118\,. \tag{4}$$

Thus, the lower end of the range of the airborne fraction f is about 0.12 (given by Eq. 4), while the upper end of the range might be derived from modern anthropogenic fossil fuel emissions to about 0.45 (Le Quéré et al., 2009). Please note that f estimated with Eq. (4) assumes a passive (constant) terrestrial biosphere, while in the estimate of f from fossil fuel emissions (Le Quéré et al., 2009), the terrestrial carbon cycle is assumed to take up about a third of the anthropogenic C emissions. We take the range of f between 0.12 and 0.45 as a first order approximation and assume f during the B/A to lie in-between. This implies that a long-term rise in atmospheric CO_2 of 10 ppmv (equivalent to a rise in the atmospheric C reservoir by 21.2 Pg C) can be generated by the injection of 47 to 180 Pg C into the atmosphere.

We further refine this amplitude to 125 Pg C (equivalent to $f = 0.17$) by using the global carbon cycle box model BICYCLE. The model then generates atmospheric CO_2 peaks of 20–35 ppmv, depending on the abruptness of the C injection (Fig. 4a). All scenarios with release times of 50–200 yr fulfil the EDC ice core data requirements after the application of the age distribution PDF (Fig. 4b). The acceptable scenarios imply rates of change in atmospheric CO_2 of 13–70 ppmv per century, a factor of 3–16 higher than in the EDC data. Our fastest scenario (release time of 50 yr) has a rate of change in atmospheric CO_2, which is still a factor of two smaller than the anthropogenic CO_2 rise of 70 ppmv during the last 50 yr (Keeling et al., 2009). For comparison, in the less precise CO_2 data points taken from the Taylor Dome (Smith et al., 1999) and Siple Dome (Ahn et al., 2004) ice cores, the abrupt rise in CO_2 at the onset of the B/A is recorded with 15±2 and 19±4 ppmv, respectively (Fig. 4a), with changing rates in ice core CO_2 of ∼4–6 ppmv per century. This already indicates that at 14.6 kyr BP, CO_2 measured in-situ in EDC differed markedly from the true atmospheric CO_2.

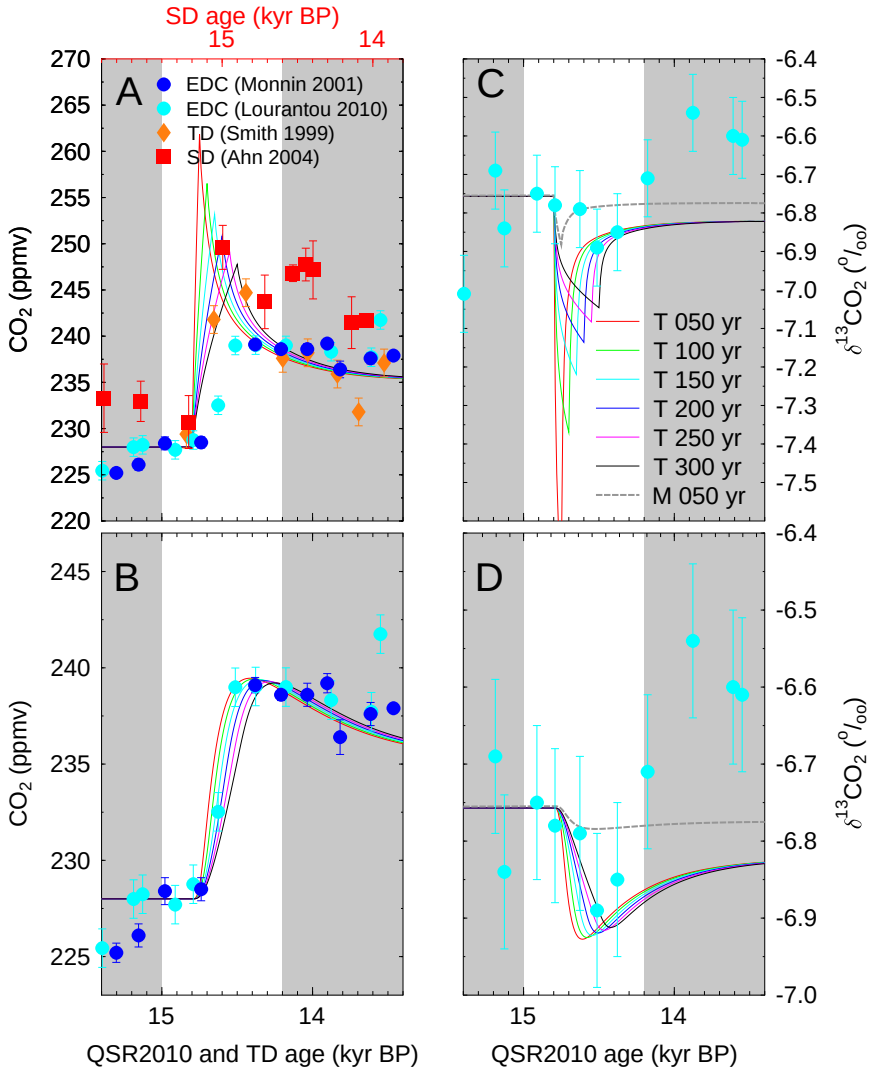

Fig. 4. Simulations with the carbon cycle box model BICYCLE for an injection of 125 Pg C into the atmosphere. Injected carbon was either of terrestrial (T: δ^{13}C=−22.5‰) or marine (M: δ^{13}C=−8.5‰) origin. Release of terrestrial C occurred between 50 and 300 yr. Marine C was released in 50 yr (grey), but is identical to the terrestrial release in A, B. **(A)** Atmospheric CO_2 from simulations and from EDC (Monnin et al., 2001; Lourantou et al., 2010) on the new age scale QSR2010 (Lemieux-Dudon et al., 2010), Siple Dome (Ahn et al., 2004) (SD, on its own age scale on top x-axis) and Taylor Dome (Smith et al., 1999) (TD, on revised age scale as in Ahn et al., 2004). All CO_2 data has been synchronised to the CO_2 jump. **(B)** Simulated CO_2 values potentially be recorded in EDC and EDC data. The simulated values are derived by the application of the gas age distribution PDF of the hypothetical atmospheric CO_2 values plotted in (A), followed by a shift in the age scale by the width $E_{B/A} = 400$ yr towards younger ages. **(C, D)** The same simulations for atmospheric $\delta^{13}CO_2$, cyan dots are new EDC $\delta^{13}CO_2$ data (Lourantou et al., 2010). Only the dynamics between 15.0 and 14.2 kyr BP (white band) are of interest here and should be compared to the ice core data.

The uncertainty in the size of the CO_2 peak given by the variability in the width $E_{B/A}$ of the age distribution PDF and by the range in the airborne fraction f lead to slightly different results. The differences in $E_{B/A}$ between 320 and 480 yr give for $f = 0.17$ variations in the atmospheric CO_2 peak height of less than 1 ppmv from the standard case and these results are still within uncertainties of the ice core data (Fig. 5b). We show in Fig. 5a and 5c how the atmospheric CO_2 and $\delta^{13}CO_2$ would look like for the upper ($f = 0.45$) and lower ($f = 0.12$) end-of-range values in the airborne fraction f, if simulated with our carbon cycle box model using a release time of 100 yr. The signal potentially recorded in EDC is achieved after applying the age distribution PDF (Fig. 5b, 5d). Atmospheric CO_2 rose by 10 ppmv only in the 47 Pg C-scenario, which would potentially be recorded as 4 ppmv in EDC. In the 180 Pg C-scenario the CO_2 amplitude

in the atmosphere would be 42 ppmv, which is 13 ppmv larger than the 29 ppmv in our reference case, leading to a long-term CO_2 jump of 16 ppmv in a hypothetical EDC ice core. After the application of the age distribution PDF, both extreme cases for f were not in line with the evidence from the ice core data.

3.2 Fingerprint analysis and process detection – the shelf flooding hypothesis

But what generated this jump of CO_2 at the onset of the B/A? Changes in the near-surface temperature and in the AMOC had massive impacts on the reorganisation of the terrestrial and the marine carbon cycle (Köhler et al., 2005b; Schmittner and Galbraith, 2008), respectively. This led to CO_2 amplitudes of about 20 ppmv during D/O events (Ahn and Brook, 2008). At the onset of the B/A the temperature changes in the northern and southern high latitudes as recorded in Greenland and in the central Antarctic plateau followed the typical pattern of the bipolar seesaw that also characterised the last glacial cycle (EPICA-community-members, 2006; Barker et al., 2009): gradual warming in the South during a stadial cold phase in the North switched to gradual cooling at the onset of a abrupt temperature rise in the North (Fig. 1a). These interhemispheric patterns were identified for all D/O events during Marine Isotope Stage 3 (MIS 3) and for the B/A as D/O event 1 (EPICA-community-members, 2006) (Fig. 1). In contrast to all D/O events during MIS 3, in which CO_2 started to decline at the onset of Greenland warming (Ahn and Brook, 2008), CO_2 abruptly increased around 14.6 kyr BP. This temporal pattern strongly suggests that changes in the AMOC are not the main source of the detected CO_2 jump at the onset of the B/A, since the general trend of the CO_2 evolution during the D/O events in MIS 3 is, based on existing data, of opposite sign.

However, we have to acknowledge that the mean temporal resolution Δt of CO_2 data obtained from various other ice cores in MIS 3 is with $\Delta t = 150$–1000 yr much larger than for the CO_2 record of EDC during Termination I ($\Delta t = 92$ yr, Table 1). For this comparison, one needs to consider that those data with the highest temporal resolution (Byrd, $\Delta t = 150$ yr, Neftel et al., 1988) are those with the highest measurement uncertainty (mean $1\sigma = 4$ ppmv, for comparison EDC: mean $1\sigma \leq 1$ ppmv). All other CO_2 ice core records in MIS 3 have $\Delta t > 500$ yr. Furthermore, present day accumulation rates in these other ice cores are 2–5 times higher than in EDC, implying an approximately 2–5 times lower mean width E of the gas age distribution PDF in the other ice cores (Spahni et al., 2003) and thus a smaller smoothing effect of the gas enclosure (Table 1). Therefore, the possibility that similar abrupt CO_2 rises in the true atmospheric signal also exist during other D/O events can not be excluded, although the data evidence from the overlapping CO_2 records of the Taylor Dome and Byrd ice cores does not seem to allow such dynamics for the time between 20–47 kyr BP (Table 1, Ahn and Brook, 2007). Furthermore, the rate of change in CO_2 at the onset of the B/A is not unique for the last glacial cycle. In the time window 65–90 kyr, BP (belonging to MIS 4 and 5) CO_2 measured in-situ in the Byrd ice core (Ahn and Brook, 2008) rose several times abruptly by up to 22 ± 4 ppmv in 200 yr, sometimes synchronous with northern warming (similar as for the B/A), and sometimes not. It needs to be tested if a similar mechanism as proposed here was also responsible for these CO_2 jumps. An ice core with higher resolution, e.g. the West Antarctic Ice Sheet (WAIS) Divide Ice Core, might help to clarify the magnitude and shape of the abrupt rise in atmospheric CO_2 during the onset of the B/A and its uniqueness with respect to other D/O events in MIS 3. The WAIS Divide Ice Core exhibits a present day accumulation rate of $24\,g\,cm^{-2}\,yr^{-1}$ (Morse et al., 2002), which is nearly an order of magnitude larger than EDC and 50% larger than Byrd (Table 1).

Our working hypothesis also implies that the changes in the AMOC connected with the bipolar seesaw pattern observed for B/A and other D/O events during MIS 3 were similar. Proxy-based evidence supports this assumed similarity: A reduction of the AMOC to a similar strength during various stadials (Younger Dryas, Heinrich Stadials 1 and 2) was deduced from $^{231}Pa/^{230}Th$ (McManus et al., 2004; Lippold et al., 2009). These results were also supported by reconstructed ventilation ages in the South Atlantic off the coast of Brazil (Mangini et al., 2010). The magnitude of the AMOC amplification during a stadial/interstadial transition is more difficult to deduce from proxy data. However, Barker et al. (2010) recently reconstructed ventilation changes in the South Atlantic Ocean and found a deep expansion of the North Atlantic Deep Water export during the B/A (following Heinrich Stadial 1), similar to results during the D/O event 8 around 38 kyr BP (following Heinrich Stadial 4). Taken together the data-based evidence indicates that (a) the AMOC was shut down in a very similar way during Heinrich Stadials, and (b) the magnitude and the characteristics of the AMOC amplification at the B/A was not exceptional (Knorr and Lohmann, 2007; Barker et al., 2010). Thus, the AMOC amplification during the B/A seemed to be similar to some D/O events in MIS 3 following Heinrich Stadials. Both indications support our assumption that changes in the AMOC can not explain the majority of the abrupt rise in atmospheric CO_2 at the onset of the B/A. The robustness of our hypothesis with respect to the uniqueness of the event might also be tested by future higher resolved CO_2 data, as mentioned above.

To constrain the origin of the released carbon further, we investigate the two hypotheses, that the carbon was only of either terrestrial or marine origin. Our two scenarios vary only in the isotopic signature of the injected C (terrestrial: $\delta^{13}CO_2$=−22.5‰, marine: $\delta^{13}CO_2$=−8.5‰). We compare carbon cycle model simulations of the typical fingerprint of these two hypotheses with new measurements of atmospheric $\delta^{13}CO_2$ from EDC (Lourantou et al., 2010). We find that the

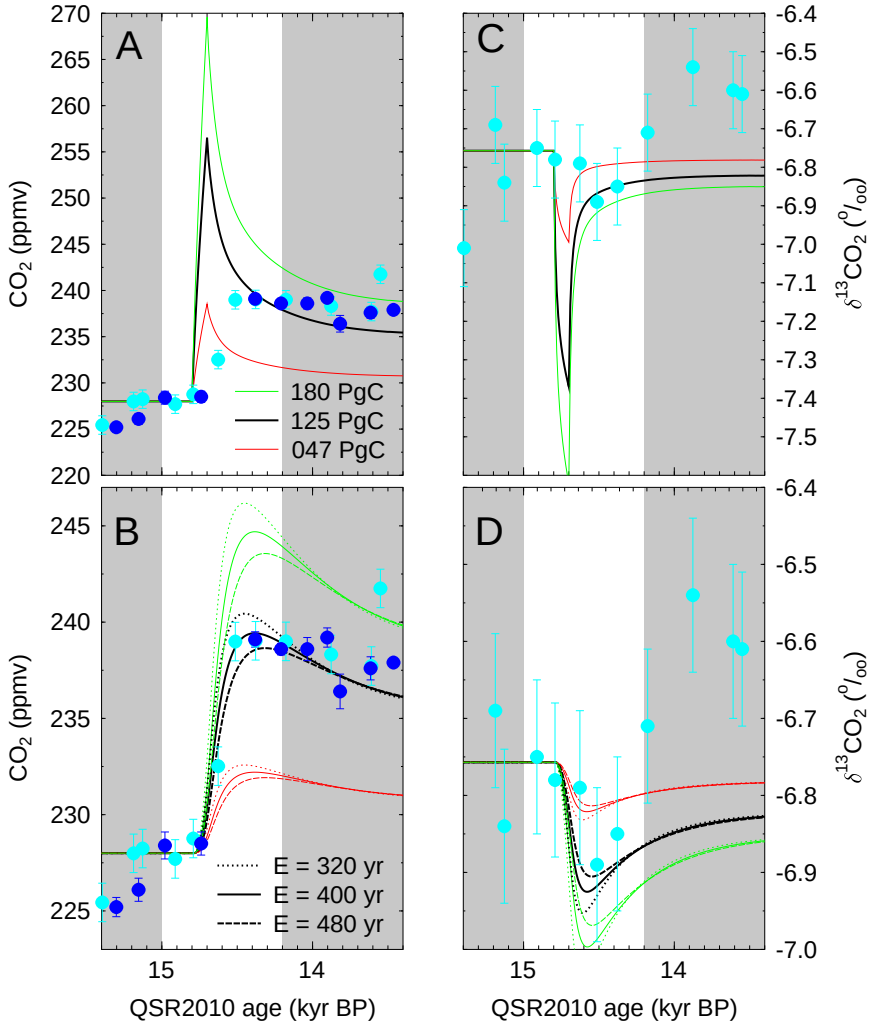

Fig. 5. Influence of (i) the amount of carbon injected in the atmosphere and of (ii) the details of the gas age distribution on both the atmospheric signal and that potentially recorded in EDC. The amount of carbon injected in the atmosphere **(A, C)** covers the range derived from an airborne fraction f between 12 and 45% from 47 to 180 Pg C with our reference scenario of 125 Pg C in bold. Injections occurred in 100 yr with terrestrial δ^{13}C signature. In the filter function of the gas age distribution **(B, D)** the width E varies from 320 yr to 480 yr, our best-estimated gas age width E at the onset of the B/A of 400 yr in the solid line, representing the range given by the firn densification model including heat diffusion (Goujon et al., 2003), as plotted in Fig. 3. Only the dynamics between 15.0 and 14.2 kyr BP (white band) are of interest here and should be compared with the ice core data.

small dip of -0.14 ± 0.14‰ in $\delta^{13}CO_2$ measured in-situ in EDC might be generated by terrestrial C released in less than three centuries (Fig. 4c, 4d). The marine scenario leads to changes in $\delta^{13}CO_2$ of less than -0.03‰ (Fig. 4d). Within the uncertainty in so-far-published ice core $\delta^{13}CO_2$ of 0.10‰ (1σ), this marine scenario seems less likely than the terrestrial one, but it can not be excluded. All together, this $\delta^{13}CO_2$ fingerprint analysis shows that all terrestrial or marine scenarios seemed to be possible, but a further constraint is, based on the given data so far, not possible. New measured, but up to now unpublished $\delta^{13}CO_2$ data does not seem to lead to different conclusions (Fischer et al., 2010).

Besides the similarity in the typical patterns of the bipolar seesaw, the B/A and the other D/O events differ significantly in the rate of sea level rise. While the amplitudes of sea level variations are with about 20 m during MIS 3 and B/A comparable (Peltier and Fairbanks, 2007; Siddall et al., 2008), the rates of change are not. It took one to several millennia for the sea level to change during MIS 3 (rate of change of 1–2 m per century, Siddall et al., 2008), but during MWP-1A the sea level rose by more than 5 m per century accumulating 16 to 20 m of sea level rise within centuries (Peltier and Fairbanks, 2007; Hanebuth et al., 2000). The exact magnitude but also the timing of the sea level rise during MWP-1A

Table 1. Available high resolution ice core CO_2 records over the last glacial cycle in comparison to the EPICA Dome C data covering Termination I.

ice core	time window	#	mean Δt	present day acc. rate*	CO_2 mean 1σ	reference
units	kyr BP	–	yr	g cm^{-2} yr^{-1}	ppmv	
EPICA Dome C	10–20	109	92	3	≤ 1	Monnin et al. (2001); Lourantou et al. (2010)
Taylor Dome	20–60	73	550	7	≤ 1	Indermühle et al. (2000)
Siple Dome	20–41	21	1000	12	2	Ahn et al. (2004)
Byrd	30–47	113	150	16	4	Neftel et al. (1988) as published in Ahn and Brook (2007)
Byrd	47–65	34	530	16	2	Ahn and Brook (2007)
Byrd	65–91	76	342	16	2	Ahn and Brook (2008)

* Taken from the compilation of Ahn et al. (2004).

varied depending on site location and reconstruction method. However, Sunda Shelf data (Hanebuth et al., 2000; Kienast et al., 2003) and recent evidence from Tahiti (Deschamps et al., 2009) point to a timing of MWP-1A at 14.6 kyr BP, in parallel to the temperature rise and the abrupt rise in CO_2 at the onset of the B/A. Sea level records (Thompson and Goldstein, 2007) suggest that large shelf areas which were exposed around 30 kyr BP were re-flooded within centuries by MWP-1A. The terrestrial ecosystems had thus ample time to develop dense vegetation and accumulate huge amounts of carbon, which could thus be released abruptly. In contrast to MWP-1A, the gradual sea level rise during MIS 3 allowed for CO_2 equilibration between atmosphere and ocean. This difference between the B/A and other D/O events in MIS 3 in both the rate of sea level rise and the return interval of shelf flooding events (used for terrestrial carbon build-up) suggests that other rapid CO_2 jumps are probably not caused by the process of shelf flooding.

We estimate from bathymetry (Smith and Sandwell, 1997, version 12.1) that 2.2, 3.2 or 4.0×10^{12} m^2 of land were flooded during MWP-1A for sea level rising between -96 m and -70 m by 16, 20 or 26 m, respectively. This covers the different reconstructions published for MWP-1A (from -96 m to -80 m, from -90 m to -70 m, or a combination of both, Hanebuth et al., 2000; Peltier and Fairbanks, 2007). It ignores differences in sea level rise due to local effects such as continental uplift or subduction, glacio-isostasy and the relative position with respect to the entry point of waters responsible for MWP-1A. About 23% of the flooded areas (Fig. 6) are located in the tropics (20° S to 20° N). To calculate the upper limit of the amount of carbon potentially released by shelf flooding during MWP-1A, we assume present-day carbon storage densities typical for tropical rain forests (60 kg m^{-2}) for the tropical belt, and the global mean (20 kg m^{-2}) for all other areas (Sabine et al., 2004b). Depending on the assumed sea level rise mentioned above, we estimate that up to 64, 94 or 116 Pg C (equivalent to 51 to 93% of the necessary C injection) might have been stored on those lands flooded during MWP-1A with about 50% located in the tropical belt. This estimate includes a complete relocation of the carbon stored on the flooded shelves to the atmosphere without any significant time delay. The efficiency of this "flooding-scenario" depends on the relative timing of MWP-1A. Several studies have indicated a time window between the onset of the B/A and the Older Dryas, i.e. between about 14.7 and 14 kyr BP (Stanford et al., 2006, 2011; Hanebuth et al., 2000; Kienast et al., 2003; Peltier and Fairbanks, 2007), including scenarios that place MWP-1A right at the onset of the B/A (Hanebuth et al., 2000; Kienast et al., 2003; Deschamps et al., 2009).

To set the timing of the abrupt rise in atmospheric CO_2 into the temporal context with MWP-1A one has to consider that the recent ice core age model used here (Lemieux-Dudon et al., 2010) is based on the synchronisation of CH_4 measured in-situ in various ice cores. Accounting for a similar age distribution PDF in CH_4 than in CO_2, the abrupt CH_4 rise at the onset of the B/A is recorded in EDC about 200 yr later than in the Greenland ice core NGRIP, which depicts the atmospheric CH_4 signal with only a very small temporal offset, due to its high accumulation rate (Appendix B, Supplement). If corrected for this CH_4 synchronisation artefact, the proposed atmospheric rise in CO_2 then starts around 14.6 kyr BP, in perfect agreement with the possible dating of MWP-1A (Fig. 7).

The residual carbon needs to be related to other processes. From the discussed comparison of the B/A with other D/O events during MIS 3, it has emerged that processes directly related to the bipolar temperature seesaw (e.g. enhanced northern hemispheric soil respiration due to warming or vegetation displacements (Köhler et al., 2005b), marine productivity changes (Schmittner and Galbraith, 2008) connected with changes in the AMOC) are unlikely candidates, because they should also have been in operation during those other D/O events and would then have led to a similar carbon release. However, it might certainly be possible that the amplification strength of the AMOC, and thus the bipolar seesaw, varied between different D/O events and thus a minor fraction of the released carbon might have been related to such

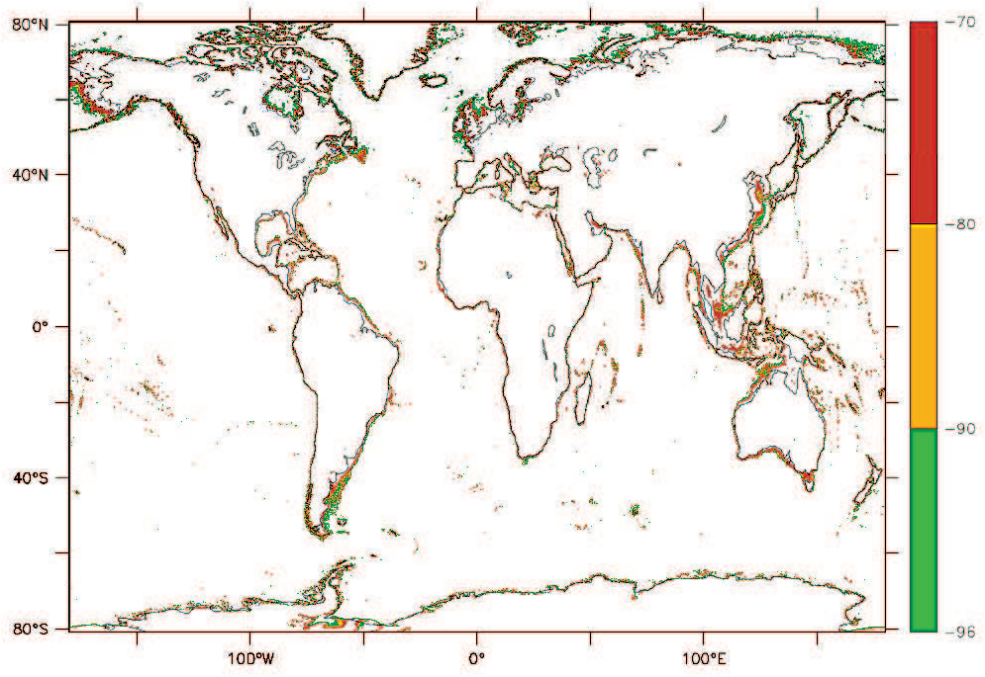

Fig. 6. Areas flooded during MWP-1A. Changes in relative sea level from −96 m to −70 m are plotted from the most recent update (version 12.1) of a global bathymetry (Smith and Sandwell, 1997) with 1 min spatial resolution ranging from 81° S to 81° N.

processes. The origin of the water masses responsible for MWP-1A is debated (Peltier, 2005). If a main fraction of the waters was of northern origin and released during a retreat (not a thinning) of northern hemispheric ice sheets, then the release of carbon potentially buried underneath ice sheets following the glacial burial hypothesis (Zeng, 2007) might also be considered. This might, however, be counteracted by enhanced carbon sequestration on new land areas available at the southern edge of the retreating ice sheets. Both processes are irrelevant for the retreating ice sheets in Antarctica. The generation of new wetlands at the onset of the B/A, as corroborated by the isotopic signature of $\delta^{13}CH_4$ points to a unique redistribution of the land carbon cycle during that time (Fischer et al., 2008). Furthermore, a potential contribution from the ocean might also be necessary. However, a quantification of these processes is not in the scope of this study.

3.3 The impact of shelf flooding on the carbon cycle

Shelf flooding might have had an impact on the marine export production. According to Rippeth et al. (2008), the flooding of continental shelves would have increased the marine biological carbon pump. This hypothesis is based on recent observations that shelf areas are sinks for atmospheric CO_2 (e.g. Thomas et al., 2005a,b). Thus, increasing the area of flooded shelves by sea level rise would according to Rippeth et al. (2008) increase the marine net primary production and might lead to enhanced export production and reduced atmospheric CO_2. The impact of shelf flooding on the marine export production might therefore have increased the amplitude of the atmospheric CO_2 rise, which needs to be explained by other processes.

To our knowledge, so far no study considers how carbon stored on land would be released in detail by flooding events. Our first order approximation given here is therefore based on the assumption that all carbon stored on land is released into the atmosphere within the given time window of the carbon injection (50 to 200 yr). Our understanding of shelf flooding is as follows: a rise in sea level with a rate of more than 5 m per century typical for MWP-1A would be superimposed on sea level variability with higher frequencies (e.g. tides). Short sea level high stands (e.g. spring tides) successively threaten plants so far established on the flooded land. Salt-intolerant species would be the first to suffer and become locally extinct after sufficient exposure to salt-water conditions, even after a temporal water retreat following sea level high stands. Finally, all previously established plants relying on freshwater conditions would die and decay. The decay of foliage is abrupt (less than a 1 yr), while that of hard wood might takes considerably longer (up to 10 yr in recent Amazonian rain forest plots, Chao et al., 2009). Heterotrophic respired carbon of this dead vegetation is dominantly partitioned to the detritus and partially to the atmosphere and soil pools. Detritus itself has a turn over times of a few years only. Most soil carbon pools have a turnover time of less than one century. We therefore assume that after the collapse of the vegetation, implying a stop to the

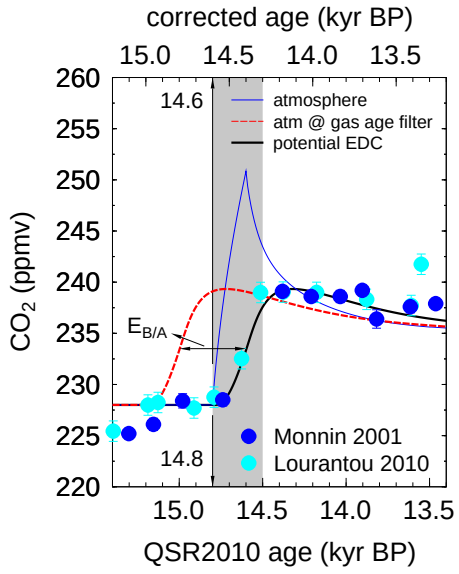

Fig. 7. Influence of the gas age distribution PDF on the CO_2 signal. The original atmospheric signal (blue) leads to a time series (red) with similar characteristics (e.g., mean values) after filtering with the gas age distribution PDF with the width $E_{B/A} = 400$ yr. To account for the use of the width of the gas age PDF in the gas chronology (R. Spahni, personal communication, 2010) the resulting curve has to be shifted by $E_{B/A}$ towards younger ages to a time series potentially recorded in EDC (black). This leads to a synchronous start in the CO_2 rise in the atmosphere (blue) and in EDC (black) around 14.8 kyr BP on the ice core age scale QSR2010 (lower x-axis) (Lemieux-Dudon et al., 2010). Due to a similar gas age distribution PDF of CH_4 the synchronisation of ice core data contains a dating artefact which is for EDC at the onset of the B/A around 200 yr (Appendix B, Supplement). On the age scale corrected for the synchronisation artefact (upper x-axis), the onset in atmospheric CO_2 falls together with the earliest timing of MWP-1A (grey band) (Hanebuth et al., 2000; Kienast et al., 2003).

input of carbon into the soil carbon pools, most soil carbon is released into the atmosphere in less than a century. Our estimate that 50% of the released carbon had originated in the tropics would allow for an even faster release of terrestrial carbon into the atmosphere, because respiration rates are temperature dependent and much faster (turnover times much smaller) in the warm and humid tropics than in boreal regions. The soil carbon release is affected by rising sea level and thus salt water conditions and depends on the temporal offset between the vegetation collapse and the start of the long-term influence of salty water on the soil. Following the spring tide idea above, this temporal offset might have been substantial, e.g. some decades. All together, the carbon released from flooded shelves might include nearly the complete standing stocks and should not be delayed by more than a century.

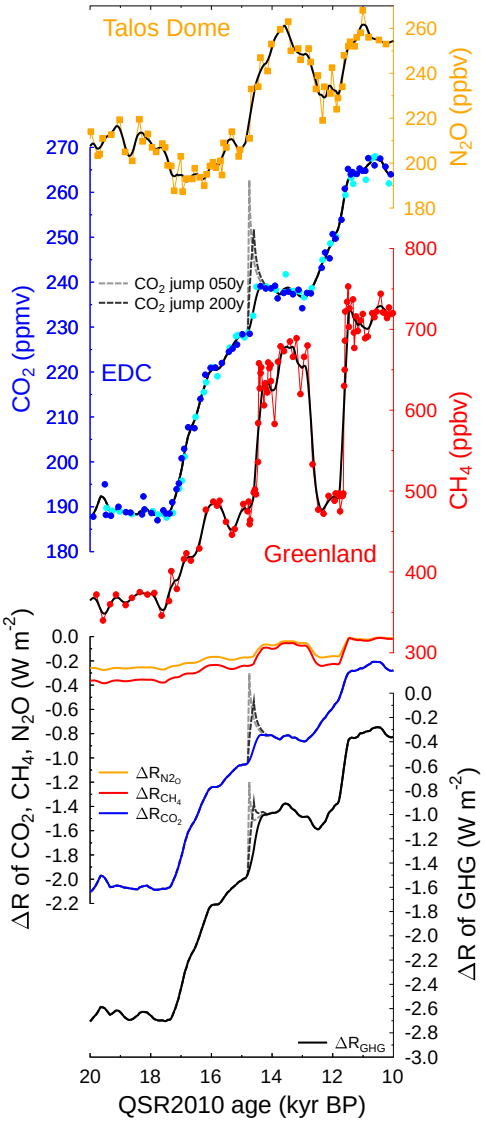

Fig. 8. Greenhouse gas records (Talos Dome N_2O, EDC CO_2, Greenland composite CH_4) and their radiative forcing ΔR during Termination I. See Captions to Fig. 1b for details. EDC CO_2 and Greenland composite CH_4 are plotted on the QSR2010 age scale, thus without considering a potential dating artefact in EDC CO_2 due to CH_4 synchronisation, Talos Dome N_2O is shown on the TALDICE-1 age scale. Black lines are running means over 290 yr (to reduce sampling noise) of resamplings with 10 yr equidistant spacing. Talos Dome and Greenland gas records are temporally higher resolved than EDC and should contain a much smaller effect of the age distribution PDF proposed for CO_2 in EDC. The two CO_2 jump scenarios are the minimum and maximum injection scenarios from our BICYCLE simulations which are still in line with the in-situ CO_2 data in EDC. The 50-yr and 200-yr injection scenario contains a constant injection flux of either 2.5 and 0.625 Pg C yr^{-1}, respectively, over the given time window. The calculated radiative forcing ΔR uses equations summarised in Köhler et al. (2010a) including a 40% enhancement of the effect of methane (Hansen et al., 2008).

4 Conclusions

Our analysis provides evidence that changes in the true atmospheric CO_2 at the onset of the B/A include the possibility of an abrupt rise by 20–35 ppmv within less than two centuries. This result depends in its details on the applied model and the assumed carbon injection scenarios and needs further investigations into sophisticated carbon cycle-climate models, because the radiative forcing of this CO_2 jump alone is 0.59–0.75 $W m^{-2}$ in 50–200 yr (Fig. 8). The Planck feedback of this forcing causes a global temperature rise of 0.18–0.23 K, which other feedbacks would amplify substantially (Köhler et al., 2010a). Based on the dynamical linkage between the temperature rise, the changes in the AMOC and the timing of MWP-1A we have provided a shelf flooding hypothesis which might explain the CO_2 jump at the onset of the B/A. In the light of existing CO_2 data, this dynamic is distinct from the CO_2 signature during other D/O events in MIS 3 and might potentially define the point of no return during the last deglaciation. A new CO_2 record from the WAIS Divide ice core has the potential to clarify whether this abrupt rise in atmospheric CO_2 during the B/A is unique with respect to other D/O events during the last 60 kyr, thus also testing the robustness of our hypothesis. The mechanism of continental shelf flooding might also be relevant for future climate change, given the range of sea level projections in response to rising global temperature and potential instabilities of the Greenland and the West Antarctic ice sheets (Lenton et al., 2008). In analogy to the identified deglacial sequence, such an instability might amplify the anthropogenic CO_2 rise.

Supplementary material related to this article is available online at: http://www.clim-past.net/7/473/2011/cp-7-473-2011-supplement.pdf.

Acknowledgements. We thank Hubertus Fischer for discussions and for pointing us at the question of strong terrestrial carbon changes during abrupt CO_2 jumps. Johannes Freitag provided us with insights to gases in firn and related difficulties in dating ice core gas records. Renato Spahni provided the gas age distribution calculated with a firn densification model plotted in Fig. 2 and in-depth details on gas chronologies. We thank Luke Skinner, Mark Siddall and an anonymous reviewer for their constructive comments. Work done at LGGE was partly funded by the LEFE programme of Institut National des Sciences de l'Univers.

Edited by: L. Skinner

References

Ahn, J. and Brook, E. J.: Atmospheric CO_2 and climate from 65 to 30 ka B.P., Geophysical Research Letters, 34, L10703, doi:10.1029/2007GL029551, 2007.

Ahn, J. and Brook, E. J.: Atmospheric CO_2 and climate on millennial time scales during the last glacial period, Science, 322, 83–85, doi:10.1126/science.1160832, 2008.

Ahn, J., Wahlen, M., Deck, B. L., Brook, E. J., Mayewski, P. A., Taylor, K. C., and White, J. W. C.: A record of atmospheric CO_2 during the last 40,000 years from the Siple Dome, Antarctica ice core, J. Geophys. Res., 109, D13305, doi:10.1029/2003JD004415, 2004.

Barker, S., Diz, P., Vantravers, M. J., Pike, J., Knorr, G., Hall, I. R., and Broecker, W. S.: Interhemispheric Atlantic seesaw response during the last deglaciation, Nature, 457, 1007–1102, doi:10.1038/nature07770, 2009.

Barker, S., Knorr, G., Vautravers, M. J., Diz, P., and Skinner, L. C.: Extreme deepening of the Atlantic overturning circulation during deglaciation, Nature Geoscience, 3, 567–571, doi:10.1038/ngeo921, 2010.

Buiron, D., Chappellaz, J., Stenni, B., Frezzotti, M., Baumgartner, M., Capron, E., Landais, A., Lemieux-Dudon, B., Masson-Delmotte, V., Montagnat, M., Parrenin, F., and Schilt, A.: TALDICE-1 age scale of the Talos Dome deep ice core, East Antarctica, Clim. Past, 7, 1–16, doi:10.5194/cp-7-1-2011, 2011.

Chao, K.-J., Phillips, O. L., Baker, T. R., Peacock, J., Lopez-Gonzalez, G., Vásquez Martínez, R., Monteagudo, A., and Torres-Lezama, A.: After trees die: quantities and determinants of necromass across Amazonia, Biogeosciences, 6, 1615–1626, doi:10.5194/bg-6-1615-2009, 2009.

Collatz, G. J., Berry, J. A., and Clark, J. S.: Effects of climate and atmospheric CO_2 partial pressure on the global distribution of C_4 grasses: present, past and future, Oecologia, 114, 441–454, 1998.

Deschamps, P., Durand, N., Bard, E., Hamelin, B., Camoin, G., Thomas, A., Henderson, G., and Yokoyama, Y.: Synchroneity of Meltwater Pulse 1A and the Bolling onset: New evidence from the IODP Tahiti Sea-Level Expedition, Geophysical Research Abstracts, 11, EGU22 009–10 233, 2009.

EPICA-community-members: One-to-one coupling of glacial climate variability in Greenland and Antarctica, Nature, 444, 195–198, doi:10.1038/nature05301, 2006.

Fischer, H., Behrens, M., Bock, M., Richter, U., Schmitt, J., Loulergue, L., Chappellaz, J., Spahni, R., Blunier, T., Leuenberger, M., and Stocker, T. F.: Changing boreal methane sources and constant biomass burning during the last termination, Nature, 452, 864–867, doi:10.1038/nature06825, 2008.

Fischer, H., Schmitt, J., Schneider, R., Elsig, J., Lourantou, A., Leuenberger, M., Stocker, T. F., Köhler, P., Lavric, J., Raynaud, D., and Chappellaz, J.: New ice core records on the glacial/interglacial change in atmospheric $\delta^{13}CO_2$, AGU, Fall Meet. Suppl., Abstract C23D-06,13–17 December 2010, San Francisco, USA, 2010.

Goujon, C., Barnola, J.-M., and Ritz, C.: Modeling the densification of polar firn including heat diffusion: Application to close-off characteristics and gas isotopic fractionation for Antarctica and Greenland sites, J. Geophys. Res., 108, 4792, doi:10.1029/2002JD003319, 2003.

Hanebuth, T., Stattegger, K., and Grootes, P. M.: Rapid Flooding

of the Sunda Shelf: A Late-Glacial Sea-Level Record, Science, 288, 1033–1035, doi:10.1126/science.288.5468.1033, 2000.

Hansen, J., Sato, M., Kharecha, P., Beerling, D., Berner, R., Masson-Delmotte, V., Pagani, M., Raymo, M., Royer, D. L., and Zachos, J. C.: Target atmospheric CO_2: Where should humanity aim?, The Open Atmospheric Science Journal, 2, 217–231, doi:10.2174/1874282300802010217, 2008.

Indermühle, A., Monnin, E., Stauffer, B., and Stocker, T. F.: Atmospheric CO_2 concentration from 60 to 20 kyr BP from the Taylor Dome ice core, Antarctica, Geophys. Res. Lett., 27, 735–738, 2000.

Joos, F. and Spahni, R.: Rates of change in natural and anthropogenic radiative forcing over the past 20,000 years, P. Natl. Acad. Sci. USA, 105, 1425–1430, doi:10.1073/pnas.0707386105, 2008.

Keeling, R. F., Piper, S., Bollenbacher, A., and Walker, J.: Atmospheric CO_2 records from sites in the SIO air sampling network, in: Trends: A Compendium of Data on Global Change., Carbon Dioxide Information Analysis Center, Oak Ridge National Laboratory, US Department of Energy, Oak Ridge, Tenn., USA, 2009.

Kienast, M., Hanebuth, T., Pelejero, C., and Steinke, S.: Synchroneity of meltwater pulse 1a and the Bølling warming: New evidence from the South China Sea, Geology, 31, 67–70, doi:10.1130/0091-7613(2003)031<0067:SOMPAT>2.0.CO;2, 2003.

Knorr, G. and Lohmann, G.: Rapid transitions in the Atlantic thermohaline circulation triggered by global warming and meltwater during the last deglaciation, Geochem. Geophy. Geosy., 8, Q12006, doi:10.1029/2007GC001604, 2007.

Köhler, P. and Fischer, H.: Simulating changes in the terrestrial biosphere during the last glacial/interglacial transition, Global and Planetary Change, 43, 33–55, doi:10.1016/j.gloplacha.2004.02.005, 2004.

Köhler, P., Fischer, H., Munhoven, G., and Zeebe, R. E.: Quantitative interpretation of atmospheric carbon records over the last glacial termination, Global Biogeochem. Cy., 19, GB4020, doi:10.1029/2004GB002345, 2005a.

Köhler, P., Joos, F., Gerber, S., and Knutti, R.: Simulated changes in vegetation distribution, land carbon storage, and atmospheric CO_2 in response to a collapse of the North Atlantic thermohaline circulation, Clim. Dynam., 25, 689–708, doi:10.1007/s00382-005-0058-8, 2005b.

Köhler, P., Bintanja, R., Fischer, H., Joos, F., Knutti, R., Lohmann, G., and Masson-Delmotte, V.: What caused Earth's temperature variations during the last 800,000 years? Data-based evidences on radiative forcing and constraints on climate sensitivity, Quaternary Sci. Rev., 29, 129–145, doi:10.1016/j.quascirev.2009.09.026, 2010a.

Köhler, P., Fischer, H., and Schmitt, J.: Atmospheric $\delta^{13}CO_2$ and its relation to pCO_2 and deep ocean $\delta^{13}C$ during the late Pleistocene, Paleoceanography, 25, PA1213, doi:10.1029/2008PA001703, 2010b.

Kroopnick, P. M.: The distribution of ^{13}C of $\sum CO_2$ in the world oceans, Deep-Sea Res. A, 32, 57–84, 1985.

Le Quéré, C., Raupach, M. R., Canadell, J. G., Marland, G., Bopp, L., Ciais, P., Conway, T. J., Doney, S. C., Feely, R. A., Foster, P., Friedlingstein, P., Gurney, K., Houghton, R. A., House, J. I., Huntingford, C., Levy, P. E., Lomas, M. R., Majku, J., Metz, N., Ometto, J. P., Peters, G. P., Prentice, I. C., Randerson, J. T., Running, S. W., Sarmiento, J. L., Schuster, U., Sitch, S., Takahashi, T., Viovy, N., van der Werf, G. R., and Woodward, F. I.: Trends in the sources and sinks of carbon dioxide, Nature Geoscience, 2, 831–836, doi:10.1038/ngeo689, 2009.

Lemieux-Dudon, B., Blayo, E., Petit, J.-R., Waelbroeck, C., Svensson, A., Ritz, C., Barnola, J.-M., Narcisi, B. M., and Parrenin, F.: Consistent dating for Antarctic and Greenland ice cores, Quaternary Sci. Rev., 29, 8–20, doi:10.1016/j.quascirev.2009.11.010, 2010.

Lenton, T. M., Held, H., Kriegler, E., Hall, J. W., Lucht, W., Rahmstorf, S., and Schellnhuber, H. J.: Tipping elements in the Earth's climate system, P. Natl. Acad. Sci. USA, 105, 1786–1793, doi:10.1073/pnas.0705414105, 2008.

Lippold, J., Grätzner, J., Winter, D., Lahaye, Y., Mangini, A., and Christl, M.: Does sedimentary $^{231}Pa/^{230}Th$ from the Bermuda Rise monitor past Atlantic Meridional Overturning Circulation?, Geophys. Res. Lett., 36, L12601, doi:10.1029/2009GL038068, 2009.

Lloyd, J. and Farquhar, G. D.: ^{13}C discrimination during CO_2 assimilation by the terrestrial biosphere, Oecologia, 99, 201–215, 1994.

Lourantou, A., Lavrič, J. V., Köhler, P., Barnola, J.-M., Michel, E., Paillard, D., Raynaud, D., and Chappellaz, J.: Constraint of the CO_2 rise by new atmospheric carbon isotopic measurements during the last deglaciation, Global Biogeochem. Cy., 24, GB2015, doi:10.1029/2009GB003545, 2010.

Mangini, A., Godoy, J., Godoy, M., Kowsmann, R., Santos, G., Ruckelshausen, M., Schroeder-Ritzrau, A., and Wacker, L.: Deep sea corals off Brazil verify a poorly ventilated Southern Pacific Ocean during H2, H1 and the Younger Dryas, Earth Planet. Sci. Lett., 293, 269–276, doi:10.1016/j.epsl.2010.02.041, 2010.

McManus, J. F., Francois, R., Gheradi, J.-M., Keigwin, L. D., and Brown-Leger, S.: Collapse and rapid resumption of Atlantic meridional circulation linked to deglacial climate changes, Nature, 428, 834–837, 2004.

Monnin, E., Indermühle, A., Dällenbach, A., Flückiger, J., Stauffer, B., Stocker, T. F., Raynaud, D., and Barnola, J.-M.: Atmospheric CO_2 concentrations over the last glacial termination, Science, 291, 112–114, 2001.

Morse, D., Blankenship, D., Waddington, E., and Neumann, T.: A site for deep ice coring in West Antarctica: Results from aerogeophysical surveys and thermal-kinematic modeling, Ann. Glaciol., 35, 36–44, 2002.

Neftel, A., Oeschger, H., Staffelbach, T., and Stauffer, B.: CO_2 record in the Byrd ice core 50000–5000 years BP, Nature, 331, 609–611, 1988.

NorthGRIP-members: High-resolution record of Northern Hemisphere climate extending into the last interglacial period, Nature, 431, 147–151, 2004.

Oliver, K. I. C., Hoogakker, B. A. A., Crowhurst, S., Henderson, G. M., Rickaby, R. E. M., Edwards, N. R., and Elderfield, H.: A synthesis of marine sediment core $\delta^{13}C$ data over the last 150 000 years, Clim. Past, 6, 645–673, doi:10.5194/cp-6-645-2010, 2010.

Peltier, W. R.: On the hemispheric origin of meltwater pulse 1a, Quaternary Sci. Rev., 24, 1655–1671, 2005.

Peltier, W. R. and Fairbanks, R. G.: Global glacial ice volume and Last Glacial Maximum duration from an extended Barbados sea level record, Quaternary Sci. Rev., 25, 3322–3337,

doi:10.1016/j.quascirev.2006.04.010, 2007.

Rippeth, T. P., Scourse, J. D., Uehara, K., and McKeown, S.: Impact of sea-level rise over the last deglacial transition on the strength of the continental shelf CO_2 pump, Geophys. Res. Lett., 35, L24604, doi:10.1029/2008GL035880, 2008.

Sabine, C. L., Feely, R. A., Gruber, N., Key, R. M., Lee, K., Bullister, J. L., Wanninkhof, R., Wong, C. S., Wallace, D. W. R., Tilbrook, B., Millero, F. J., Peng, T.-H., Kozyr, A., Ono, T., and Rios, A. F.: The oceanic sink for anthropogenic CO_2, Science, 305, 367–371, 2004a.

Sabine, C. L., Heimann, M., Artaxo, P., Bakker, D. C. E., Arthur, C.-T., Field, C. B., Gruber, N., Le Quéré, C., Prinn, R. G., Richey, J. E., Lankao, P. R., Sathaye, J. A., and Valentini, R.: Current status and past trends of the global carbon cycle, in: The global carbon cycle: integrating humans, climate, and the natural world, edited by: Field, C. B. and Raupach, M. R., pp. 17–44, Island Press, Washington, Covelo, London, 2004b.

Schilt, A., Baumgartner, M., Schwander, J., Buiron, D., Capron, E., Chappellaz, J., Loulergue, L., Schüpbach, S., Spahni, R., Fischer, H., and Stocker, T. F.: Atmospheric nitrous oxide during the last 140,000 years, Earth Planet. Sci. Lett., 300, 33–43, doi:10.1016/j.epsl.2010.09.027, 2010.

Schmittner, A. and Galbraith, E. D.: Glacial greenhouse-gas fluctuations controlled by ocean circulation changes, Nature, 456, 373–376, doi:10.1038/nature07531, 2008.

Scholze, M., Kaplan, J. O., Knorr, W., and Heimann, M.: Climate and interannual variability of the atmosphere-biosphere $^{13}CO_2$ flux, Geophys. Res. Lett., 30, 1097, doi:10.1029/2002GL015631, 2003.

Siddall, M., Rohling, E. J., Thompson, W. G., and Waelbroeck, C.: Marine isotope stage 3 sea level fluctuations: data synthesis and new outlook, Rev. Geophys., 46, RG4003, doi:10.1029/2007RG000226, 2008.

Siegenthaler, U. and Münnich, K. O.: $^{13}C/^{12}C$ fractionation during CO_2 transfer from air to sea, in: Carbon cycle modelling, edited by Bolin, B., vol. 16 of *SCOPE*, pp. 249–257, Wiley and Sons, Chichester, NY, 1981.

Smith, H. J., Fischer, H., Wahlen, M., Mastroianni, D., and Deck, B.: Dual modes of the carbon cycle since the Last Glacial Maximum, Nature, 400, 248–250, 1999.

Smith, W. H. and Sandwell, D. T.: Global Sea Floor Topography from Satellite Altimetry and Ship Depth Soundings, Science, 277, 1956–1962, doi:10.1126/science.277.5334.1956, 1997.

Spahni, R., Schwander, J., Flückiger, J., Stauffer, B., Chappellaz, J., and Raynaud, D.: The attenuation of fast atmospheric CH_4 variations recorded in polar ice cores, Geophys. Res. Lett., 30, 1571, doi:10.1029/2003GL017093, 2003.

Spahni, R., Chappellaz, J., Stocker, T. F., Loulergue, L., Hausammann, G., Kawamura, K., Flückiger, J., Schwander, J., Raynaud, D., Masson-Delmotte, V., and Jouzel, J.: Atmospheric methane and nitrous oxide of the late Pleistocene from Antarctic ice cores, Science, 310, 1317–1321, doi:10.1126/science.1120132, 2005.

Stanford, J., Hemingway, R., Rohling, E., Challenor, P., Medina-Elizalde, M., and Lester, A.: Sea-level probability for the last deglaciation: A statistical analysis of far-field records, Global Planet. Change, doi:10.1016/j.gloplacha.2010.11.002, in press, 2011.

Stanford, J. D., Rohling, E. J., Hunter, S. E., Roberts, A. P., Rasmussen, S. O., Bard, E., McManus, J., and Fairbanks, R. G.: Timing of meltwater pulse 1a and climate responses to meltwater injections, Paleoceanography, 21, PA4103, doi:10.1029/2006PA001340, 2006.

Steffensen, J. P., Andersen, K. K., Bigler, M., Clausen, H. B., Dahl-Jensen, D., Fischer, H., Goto-Azuma, K., Hansson, M., Johnsen, S. J., Jouzel, J., Masson-Delmotte, V., Popp, T., Rasmussen, S. O., Rothlisberger, R., Ruth, U., Stauffer, B., Siggaard-Andersen, M.-L., Sveinbjörnsdóttir, A. E., Svensson, A., and White, J. W. C.: High-resolution Greenland ice core data show abrupt climate change happens in few years, Science, 321, 680–684, doi:10.1126/science.1157707, 2008.

Stenni, B., Masson-Delmotte, V., Johnsen, S., Jouzel, J., Longinelli, A., Monnin, E., Röthlisberger, R., and Selmo, E.: An oceanic cold reversal during the last deglaciation, Science, 293, 2074–2077, 2001.

Thomas, H., Bozec, Y., de Baar, H. J. W., Elkalay, K., Frankignoulle, M., Schiettecatte, L.-S., Kattner, G., and Borges, A. V.: The carbon budget of the North Sea, Biogeosciences, 2, 87–96, doi:10.5194/bg-2-87-2005, 2005a.

Thomas, H., Bozec, Y., Elkalay, K., de Baar, H. J. W., Borges, A. V., and Schiettecatte, L.-S.: Controls of the surface water partial pressure of CO_2 in the North Sea, Biogeosciences, 2, 323–334, doi:10.5194/bg-2-323-2005, 2005b.

Thompson, W. G. and Goldstein, S. L.: A radiometric calibration of the SPECMAP timescale, Quaternary Sci. Rev., 25, 3207–3206, doi:10.1016/j.quascirev.2006.02.007, 2007.

Trudinger, C. M., Etheridge, D. M., Rayner, P. J., Enting, I. G., Sturrock, G. A., and Langenfelds, R. L.: Reconstructing atmospheric histories from measurements of air composition in firn, J. Geophys. Res., 107, 4780, doi:10.1029/2001JD002545, 2002.

Zeng, N.: Quasi-100 ky glacial-interglacial cycles triggered by subglacial burial carbon release, Clim. Past, 3, 135–153, doi:10.5194/cp-3-135-2007, 2007.